Published in final edited form as:

J Cell Sci. 2008 June 1; 121(11): 1937–1949. doi:10.1242/jcs.023150.

A new model for hemoglobin ingestion and transport by the human malaria parasite *Plasmodium falciparum*

Michelle D. Lazarus, **Timothy G. Schneider**, and **Theodore F. Taraschi***

Department of Pathology, Anatomy, and Cell Biology, Thomas Jefferson University, Philadelphia, PA 19107, USA

Summary

The current model for hemoglobin ingestion and transport by intraerythrocytic *Plasmodium falciparum* malaria parasites shares similarities with endocytosis. However, the model is largely hypothetical, and the mechanisms responsible for the ingestion and transport of host cell hemoglobin to the lysosome-like food vacuole (FV) of the parasite are poorly understood. Because actin dynamics play key roles in vesicle formation and transport in endocytosis, we used the actin-perturbing agents jasplakinolide and cytochalasin D to investigate the role of parasite actin in hemoglobin ingestion and transport to the FV. In addition, we tested the current hemoglobin trafficking model through extensive analysis of serial thin sections of parasitized erythrocytes (PE) by electron microscopy. We find that actin dynamics play multiple, important roles in the hemoglobin transport pathway, and that hemoglobin delivery to the FV via the cytostomes might be required for parasite survival. Evidence is provided for a new model, in which hemoglobin transport to the FV occurs by a vesicle-independent process.

Keywords

Plasmodium; Actin; Cytostome; Food vacuole; Hemoglobin; Malaria

Introduction

There are over one hundred and sixty species of *Plasmodium*, five of which are known to infect humans. Of the human malaria parasites, *Plasmodium falciparum* causes the greatest human mortality worldwide (Francis et al., 1997), in part because of the rapidly growing resistance of the parasite to existing antimalarials (Wellems and Plowe, 2001). The malaria parasite life cycle involves two hosts. During a blood meal, a malaria-infected female *Anopheles* mosquito inoculates sporozoites into the human host. Sporozoites infect liver cells and mature into schizonts, which rupture and release merozoites. The released merozoites infect red blood cells and initiate an ~48 hour cyclical, asexual life cycle. Blood stage parasites are responsible for the clinical manifestations of the disease.

During its intraerythrocytic life cycle, the parasite is surrounded by three membranes: the parasitophorous vacuolar membrane (PVM), derived from the host erythrocyte membrane

*Author for correspondence (theodore.taraschi@jefferson.edu).

following invasion; the parasite plasma membrane (PPM); and the erythrocyte membrane. The invaded merozoite rapidly develops into the ring stage, which is marked by low metabolic activity. After ~20 hours, the parasite enters the trophozoite stage, which is marked by robust protein, RNA and DNA synthesis and the commencement of hemoglobin digestion. DNA replication occurs in the schizont stage, during which daughter merozoites are formed by asexual mitosis. Merozoites are released from the erythrocyte and initiate a new round of asexual development.

P. falciparum digests more than 80% of the erythrocyte hemoglobin to support parasite growth and asexual replication during the intraerythrocytic stage (Ginsburg, 1990; Sherman, 1977). The bulk of hemoglobin degradation occurs via a semi-ordered process by proteases contained within the lysosome-like organelle of the parasite, termed the food vacuole (FV) (Goldberg et al., 1990; Goldberg, 2005). The resulting heme is crystallized into the malarial pigment, hemozoin (Hempelmann and Egan, 2002; Slater and Cerami, 1992; Pagola et al., 2000; Scholl et al., 2005). Many antimalarials, such as chloroquine, accumulate in the acidic FV where they interfere with the hemoglobin degradation processes (Banerjee and Goldberg, 2001) and cause parasite death (Francis et al., 1997).

A prerequisite for complete hemoglobin digestion is the uptake and transport of host cell hemoglobin to the FV. Little is known, however, about the mechanisms regulating hemoglobin ingestion and transport to the parasite FV and the role this pathway plays in parasite development. Hemoglobin internalization is mediated by cytostomes (Aikawa et al., 1966; Rudzinska et al., 1965). Cytostomes are localized, double-membrane invaginations of the PPM and PVM, and are distinguished by the presence of sub-membranous, electron-dense material flanking either side of the cytostome neck (Langreth et al., 1978; Olliaro et al., 1989). Hemoglobin is proposed to be internalized by the parasite via the budding of double-membrane, cytostome-derived vesicles (Yayon et al., 1984). These vesicles are proposed to traffic to and eventually fuse with the FV. However, evidence for cytostome-derived vesicles is based on morphological interpretations of single, thin-section electron micrographs and fluorescence microscopy of parasitized erythrocytes (PE) (Aikawa et al., 1966; Dasaradhi et al., 2007; Hoppe et al., 2004; Klemba et al., 2004; Klonis et al., 2007; Langreth et al., 1978; Olliaro et al., 1989; Rudzinska et al., 1965; Yayon et al., 1984).

Biochemical characterization of the cytostomes and the associated hemoglobin transport structures is limited. Isolation of the cytostome is difficult because it is an integral part of the PVM and PPM. In addition, cytostome-specific markers are not available, which hinders the characterization of cytostome-derived transport vesicles. Because of the similarities between the current model for hemoglobin transport and the endocytic pathway in higher eukaryotes (Goldberg et al., 1990; Hoppe et al., 2004; Langreth et al., 1978; Saliba et al., 2003), we investigated the role of actin dynamics in hemoglobin transport to the FV. Actin has been shown to play various regulatory roles in endocytosis, including recruiting endocytic components to the plasma membrane, initiating plasma membrane invaginations, vesicle scission and transport to endocytic compartments (Kaksonen et al., 2006; Qualmann et al., 2000; Smythe and Ayscough, 2006). As intermediate filaments have not been identified in *P. falciparum* and microtubules do not appear until the schizont stage (Taraschi et al., 1998), well after the majority of hemoglobin internalization and degradation has occurred, we

hypothesized that actin may play a role in cytostome formation and hemoglobin transport to the FV. Although little is known about actin dynamics in intraerythrocytic stage parasites, *P. falciparum* actin (*Pf*actin) assembles as short, unstable filaments in vitro (Schmitz et al., 2005; Schuler et al., 2005). A recent report suggested a role for actin in the endocytic trafficking of hemoglobin in *P. falciparum* (Smythe et al., 2007).

Using serial-section electron microscopy and the actin-perturbing agents jasplakinolide (JAS) and cytochalasin D (CD), we evaluated the current hemoglobin transport model used by intraerythrocytic *P. falciparum*. Our results suggest that actin dynamics play key roles in cytostome organization and hemoglobin transport. We provide evidence that an alternative, vesicle-independent model is responsible for hemoglobin ingestion and transport to the FV. In addition, we demonstrate a functional link between hemoglobin transport to the FV and parasite development.

Results

Characterization of structures involved with hemoglobin internalization and transport

Morphological analysis was performed to characterize the structures and pathways involved in hemoglobin transport from the host erythrocyte cytosol to the parasite FV. Synchronized PE were analyzed by electron microscopy for the presence of cytostomes and hemoglobin-containing structures throughout the intraerythrocytic life cycle. Cytostomes were observed in the ring (0–18 hours post-invasion, Fig. 1A), trophozoite (20–32 hours post-invasion, Fig. 1B) and schizont (32–44 hours post-invasion, Fig. 1C) stages. Cytostomes were observed before FV formation (Fig. 1A) and commencement of hemoglobin digestion, which occurs at ~18–20 hours post-invasion (Gligorijevic et al., 2006; Orjih et al., 1994). The cytostomes visualized by electron microscopy in a single thin section varied in size within individual parasites (Fig. 1B,D) and between parasites (Fig. 1A–E). Multiple cytostomes were observed within single parasites and these cytostomes were often in close proximity to each other along the PVM/PPM interface (Fig. 1B,D). In some sections, the cytostomes extended through the parasite cytosol and were either closely apposed to the FV (Fig. 1B) or appeared to be inside the FV (Fig. 1C,E). Many times the cytostome and the FV membranes were indistinguishable (Fig. 1E).

We analyzed serial thin sections by electron microscopy to test empirically the vesicle-mediated hemoglobin transport model. A representative selection of serial sections through a trophozoite-stage PE is shown in Fig. 2. As was seen in Fig. 1, a PE can contain multiple cytostomes localized to specific regions of the PVM/PPM, which vary in diameter (~160 nm to ~480 nm, Fig. 2). Hemoglobin-containing structures, which appear to be discrete vesicles (Fig. 2, sections 4, 6 and 7), are in fact part of the cytostome (Fig. 2, CYT 3). We term the structures in Fig. 2, sections 4, 6 and 7, ‘cytostomal sections’ (CS), as they represent morphological sections of the cytostome. The analysis of serial sections from 72 different PE revealed that apparent hemoglobin-containing, double-membrane vesicles seen in a single parasite section, which varied between ~200 and 600 nm diameter, were always found to be part of the cytostome (data not shown).

Cytostomes are currently defined by morphological features, particularly by the presence of sub-membranous electron density at the periphery of the cytostome neck. The composition of the electron-dense material remains unknown, but its appearance and location are reminiscent of the presence of actin at the neck of caveolae (Foti et al., 2007). As visualization of actin filaments has not been described in intraerythrocytic parasites, we chose to use an electron microscopy fixative previously optimized for the visualization of actin filaments (Boyles et al., 1985). In PE prepared with 'mix-fix', the electron-dense material at the cytostome neck became more clearly defined (Fig. 3) than the morphology obtained with a more traditional fixative (Fig. 1). We discovered that the focal electron density (Fig. 1) in fact encircled the neck, and appeared in some sections to be composed of two electron-dense rings (Fig. 3C,D). Linear radiating structures were observed at the periphery of this electron-dense collar in some sections (Fig. 3B).

Actin dynamics and cytostome morphology

Although a role is emerging for *Pf*actin in merozoite invasion (Baum et al., 2006; Heintzelman, 2006; Mizuno et al., 2002), very little is known about *Pf*actin distribution and function in intraerythrocytic *P. falciparum*. Thus, we undertook an investigation to characterize *Pf*actin within PE, and to elucidate its role in the uptake of hemoglobin from the erythrocyte cytosol and subsequent transport to the parasite FV.

There is currently much dispute over the ratio of filamentous (F-actin) to globular (G-actin) within *P. falciparum* merozoites (Field et al., 1993; Schmitz et al., 2005), and the distribution of actin within intraerythrocytic-stage parasites was not investigated. We investigated actin dynamics by determining the F- (triton-insoluble) to G- (triton-soluble) actin ratios in ring (0–18 hours post-invasion), trophozoite (20–32 hours post-invasion) and schizont (32–42 hours post-invasion) stage parasites. The F- and G-actin pools were separated and analyzed by western blotting using an anti-*Toxoplasma gondii* actin antibody (Dobrowolski et al., 1997), which is reactive with *P. falciparum* but not human erythrocyte actin (Fig. 4A). Unlike most higher eukaryotes, but similar to other Apicomplexa (Dobrowolski et al., 1997), we found that the majority of *Pf*actin is maintained in the triton-soluble form, varying from greater than 90% in the ring and trophozoite stages to ~70% in the schizont stage (Fig. 4B).

We investigated the role of actin dynamics in hemoglobin transport to the FV by analyzing the effects of the actin-stabilizing agent JAS and the actin-destabilizing agent CD on PE. We focused on trophozoite stage parasites, as hemoglobin degradation commences at ~18–20 hours post-invasion and the rate of hemozoin production is greatest between 22–28 hours post-invasion (Gligorijevic et al., 2006; Orjih et al., 1994). Incubation of trophozoite stage PE with JAS increased the triton-insoluble actin pool from ~10% to 55% of the total parasite actin (compare Fig. 4B and 4C). No change in the *Pf*actin ratio was observed in trophozoite stage PE incubated with CD (compare Fig. 4B and 4C).

To spatially localize *Pf*actin in untreated and JAS- or CD-treated PE, confocal microscopy was performed. Although phalloidin is often used to visualize actin, parasite actin does not bind phalloidin in vivo (Heintzelman, 2006), and we therefore used a parasite-specific anti-actin antibody to localize *Pf*actin in PE. In untreated PE, *Pf*actin was distributed diffusely throughout the parasite cytoplasm; some *Pf*actin was also localized in punctate structures at

the parasite periphery and inside the parasite compartment (Fig. 5). CD treatment decreased the intensity of the punctate staining at the PVM/PPM but did not alter the location of diffuse staining of the parasite cytosol. By contrast, JAS treatment of trophozoites resulted in a marked redistribution of *Pf*actin from the parasite cytosol to large patches at the PVM/PPM. The fluorescence intensity at the PVM/PPM was increased compared with untreated or CD-treated PE (Fig. 5). Some *Pf*actin appeared to be exported to the host erythrocyte and was visible as punctate spots in the host cell cytosol or associated with the erythrocyte membrane. This extra-parasitic *Pf*actin was not a consequence of JAS or CD treatment as a similar pattern was observed for untreated PE (data not shown). Uninfected erythrocytes also contained some punctuate spots in the cytosol, but these were much less intense under microscopy conditions identical to those used for analyzing JAS- or CD-treated PE (data not shown).

We investigated the effects of actin-perturbing agents on cytostome morphology through the analysis of single and serial thin sections by electron microscopy. Treatment of trophozoite stage PE with either CD or JAS resulted in a 25% or 33% decrease in the number of cytostomes, respectively, compared with untreated PE (Table 1). To investigate the effects of actin-perturbing agents on cytostome structure, JAS- and CD-treated PE were analyzed using serial-section electron microscopy (Fig. 6). Serial sectioning of JAS-or CD-treated PE revealed that, similar to untreated PE (Fig. 2), the apparent discrete hemoglobin-containing compartments observed in single sections were contiguous with the cytostomes.

Cytostomes observed in PE treated with JAS (Fig. 6A) or CD (Fig. 6B) extended through more electron microscopy sections than did cytostomes observed in untreated PE (Fig. 2). In only a limited number of instances were we able to serially section completely through a cytostome in JAS- or CD-treated parasites. This suggested that cytostomes present in treated parasites were larger than those observed in untreated PE. Therefore, we developed a method using single thin-section electron micrographs to analyze the effects of the actin-perturbing drugs on PE.

An increase in cytostome size and convolution was visualized in single thin-section electron micrographs as an increase in the number of CS per parasite. The assessment that JAS or CD treatment caused the cytostomes to become more convoluted was based on the observation that cytostome number decreased concomitantly with an increase in CS number within a single thin electron micrograph section (see Tables 1 and 2). The residual cytostomes in PE treated with CD (Fig. 7B) or JAS (Fig. 7C) were larger and more convoluted than cytostomes in untreated PE (Fig. 7A). The CS in treated PE varied in size and in electron densities (Fig. 7B,C). The percentage of PE containing CS increased by 37.2% and 24.4% with CD and JAS treatment, respectively, compared with untreated PE (Table 2). Furthermore, drug treatment increased the incidence of CS per parasite by 2–3 times, with CD causing the greatest perturbation (Table 2). We do not currently know the significance of the variance in electron density within CS observed in Fig. 7B, but this phenomena was specific to CD-treated PE. In a single section, it cannot be determined whether these CS represent sections through one or more cytostomes.

Incubation of PE with JAS had profound effects on the cytostome collar. The electron density at the cytostome neck appeared to consist of two electron-dense collars that surround the neck (Fig. 8A,B; arrowheads). Radiating filaments appeared to span between the two electron-dense collars (Fig. 8C). This was especially evident in the transverse section shown in Fig. 8D, which captured the hemoglobin-filled cytostome surrounded by an electron-dense collar with electron-dense filaments extending outward into the parasite cytosol (presumably toward the second electron-dense collar).

The cytostome neck diameter was also altered following drug treatment. Table 3 provides descriptive statistics, by treatment group, in the original scale of cytostome neck diameters. Fig. 9 displays the data in the natural log scale, as used in the analysis. There was a significant difference across the untreated, CD- and JAS-treated PE groups in measured cytostome neck diameter (F-test, 2 d.f., $P<0.001$). Post-hoc paired comparisons, corrected by Tukey's HSD, indicated that JAS-treated PE have significantly larger neck diameters than do untreated or CD-treated PE, with least squares mean difference in natural log scale of 0.246 ($P<0.001$) and 0.388 ($P<0.001$), respectively. The P-value from the nonparametric analysis of variance is $P<0.001$, indicating the ANOVA results presented are robust. Additionally, neck diameters in CD-treated PE are significantly smaller than in untreated PE, with least squares mean difference of –0.142 ($P=0.042$).

Both untreated and JAS-treated PE were fixed for cryo-immuno electron microscopy and the resulting thin-section micrographs were analyzed for *Pf*actin localization (Fig. 10). A reproducible labeling pattern was difficult to discern for untreated PE. In JAS-treated PE, although the overall *Pf*actin labeling was low, there was a specific *Pf*actin labeling pattern at the PVM/PPM (Fig. 10D, arrowheads). *Pf*actin did not colocalize with all cytostomes but was observed associated with cytostome necks (Fig. 10A–C arrowheads), as well as with the cytostome body (Fig. 10A) in ~75% of PE that possessed cytostomes connected to the PVM/PPM in one thin section. Similar to our immunofluorescence data, *Pf*actin was distributed throughout the parasite cytosol (Fig. 10D, open arrowheads) and in the host cell cytosol (Fig. 10D, pointed arrowheads).

JAS treatment inhibits *P. falciparum* development and prevents hemoglobin accumulation in the FV

Our results suggested that actin dynamics are important for structural organization of the cytostome. As the cytostome is the primary source for hemoglobin ingestion by intraerythrocytic *P. falciparum* and hemoglobin catabolism has been linked to parasite survival, we investigated the effects of JAS and CD on parasite development and hemoglobin transport to the FV. Because it was previously reported that altering actin dynamics inhibited parasite invasion (Dluzewski et al., 1992; Mizuno et al., 2002; Poupel and Tardieux, 1999; Smythe at al., 2007), the effects of CD or JAS treatment on parasite development were investigated within a single intraerythrocytic cycle using a parasite lactate dehydrogenase (*Pf*LDH) assay (Goodyer and Taraschi, 1997; Makler and Hinrichs, 1993). *Pf*LDH activity increased throughout the intraerythrocytic life cycle of the parasite (Fig. 11A), thus *Pf*LDH activity can be used as a measure of parasite development.

Incubation of PE (>12 hours post-invasion) with JAS produced a statistically significant reduction in *Pf*LDH activity (Fig. 11B) compared with that of untreated PE. Inhibition of parasite development by JAS was most pronounced in parasites at the early trophozoite stage (20–24 hours post-invasion). By contrast, incubation of PE with up to 10 μM CD throughout the intraerythrocytic life cycle did not inhibit parasite development (data not shown).

These results suggested that the effects of JAS on parasite development might be due to an inhibition of the hemoglobin ingestion and/or transport pathways. We therefore investigated the effects of JAS and CD on hemoglobin translocation to the FV. We used E-64, a cysteine protease inhibitor, to indirectly measure hemoglobin accumulation in the FV. E-64 inhibits hemoglobin digestion, resulting in parasites containing swollen, electron-dense FV that are filled with undigested hemoglobin (Sijwali and Rosenthal, 2004). If JAS inhibited hemoglobin transport to the FV, then simultaneous treatment with both E-64 and JAS should prevent the E-64 phenotype by inhibiting hemoglobin translocation to the FV. PE treated with E-64 in the trophozoite stage exhibited enlarged, hemoglobin-filled FV (Fig. 12), consistent with previous reports. As these parasites were treated following the commencement of hemoglobin breakdown, some crystalline hemozoin and undigested hemoglobin was present in the FV. As expected, trophozoite stage parasites treated with JAS alone exhibited an increase in CS (Fig. 12, arrowheads), and had FV similar in appearance to those of untreated PE. The simultaneous treatment of intraerythrocytic PE with E-64 and JAS decreased the number of PE that contain swollen, electron-dense FV by 74% (Fig. 12, Table 4) compared with E-64 treated PE, suggesting that the stabilization of actin filaments inhibits hemoglobin delivery to the FV. Notably, simultaneous incubation of PE with CD and E-64 had no visible effect on the accumulation of undegraded hemoglobin in the FV (Table 4), and the FV of these PE were morphologically similar to those of PE incubated with E-64 alone (Fig. 9). Multiple CS were observed in PE treated with CD regardless of the presence of E-64 (Fig. 12).

Comparison of JAS and CD effects on PE

JAS at a concentration of ≥3.0 μM was found to perturb cytostome morphology, alter actin distribution, inhibit hemoglobin transport to the FV and inhibit parasite development. We determined that CD up to a concentration of 10 μM, which was the highest concentration we investigated, perturbed cytostome morphology and slightly altered actin distribution, but did not inhibit hemoglobin transport to the FV nor asexual development during one intraerythrocytic (44 hour) cycle.

Discussion

In this investigation, we provide evidence that actin dynamics are important at multiple steps of the cytostome-mediated hemoglobin transport pathway. In addition, our analysis of serial sections by electron microscopy provided evidence for an alternative, vesicle-independent model for hemoglobin transport from the erythrocyte cytosol to the FV. We also present evidence suggesting that hemoglobin ingestion and transport through the cytostomes to the FV may be required for parasite development.

*Pf*actin distribution and localization in intraerythrocytic stages of *P. falciparum*

Although *Pf*actin distribution and localization has been studied in invasive merozoites, little was known about *Pf*actin in the intraerythrocytic stages of *P. falciparum*. We found that the majority (>90%) of actin in intraerythrocytic PE was in the form of soluble actin (G-actin). A large, unpolymerized actin pool is observed in cells requiring rapid structural remodeling, such as in motile phagocytic neutrophils (Pollard et al., 2000). By contrast, human erythrocytes have a large F-actin pool, which largely functions to maintain the structural integrity of the cell (Pinder and Gratzer, 1983). These examples illustrate that the F- to G-actin ratio can often be indicative of the function of actin within a cell. We propose that the large triton-soluble pool implies that dynamic actin is necessary for the erythrocytic development of *P. falciparum*. This seems reasonable, as the parasite is constantly growing and modifying its encapsulating membranes, both by increasing in size and by deforming the PVM/PPM during cytostome formation. The increase in F-actin observed in schizont stage parasites may indicate a structural role for actin in the organization and organelle placement of newly formed merozoites, as is the case with microtubules (Taraschi et al., 1998).

When we characterized actin localization in unperturbed PE by immunofluorescence, an abundance of cytosolic actin was detected within the parasite compartment (Fig. 5B), consistent with our finding that the majority of actin in trophozoite stage PE was in the triton-soluble pool (Fig. 4). Some intense focal actin staining was also observed at the PVM/PPM, possibly indicative of the presence of short actin filaments (Schmitz et al., 2005). Focal actin staining was also observed in the erythrocyte cytosol of PE, suggesting that the parasite may export *Pf*actin into the host cell. We previously proposed a role for actin in the transport of parasite proteins to the host cell cytosol and surface membrane, and suggested that this actin could be of parasite origin (Taraschi et al., 2003). Although intriguing, confirmation of this process will require further investigation, as some much less intense, but similar in appearance, focal spots were also observed in the cytosol of uninfected erythrocytes under microscopy conditions identical to those used to analyze CD- or JAS-treated PE, and *Pf*actin does not appear to contain any export motif(s).

The effects of JAS and CD on actin distribution and localization in PE

To investigate the role of actin dynamics in the hemoglobin transport pathway, we used JAS and CD, both of which specifically modulate actin dynamics in eukaryotic cells (Cooper, 1987; Holzinger, 2001). These agents had different effects on the distribution of *Pf*actin within PE. JAS treatment caused both a marked increase in triton-insoluble F-actin and a striking cortical redistribution of *Pf*actin to the parasite periphery (Fig. 5B). The redistribution of actin following JAS treatment was described in other cell types, including in *T. gondii* (Bubb et al., 2000; Shurety et al., 1998; Wetzel et al., 2003). Recently, Smythe et al. also observed by immunofluorescence microscopy that treatment of PE with 1 μM JAS for 5 hours caused a cortical redistribution of actin to the parasite periphery (Smythe et al., 2007).

CD, however, did not induce a detectable change in the F- to G-actin ratio, and the actin distribution was essentially unchanged compared to that of untreated PE. CD did cause a

loss of fluorescence in a few focal areas at the PVM/PPM, as well as a small decrease in parasite cytosolic actin fluorescence (Fig. 5B). This suggests that CD might decrease actin filament length without altering the overall F- to G-actin ratio, because microfilaments can be nucleated in the presence of CD (Cooper, 1987). Similar to our results, Smythe et al. reported that actin localization in parasites incubated with 50 nM CD for 5 hours appeared indistinguishable from that of untreated PE (Smythe et al., 2007).

The role(s) of actin in cytostome structure and regulation

There are a number of parallels that can be drawn between the role of actin in endocytosis and its role in cytostome-mediated hemoglobin transport. Namely, the decrease in cytostome number and the altered cytostome morphology observed following the perturbation of actin by JAS or CD are reminiscent of the effects of perturbing actin dynamics on clathrin-coated pits (Lamaze et al., 1997; Yarar et al., 2005). Clathrin-coated pits decreased in number and were more deeply invaginated when actin dynamics were perturbed. The decrease in cytostome number suggests that actin may play a role early in cytostome formation, as no change or an increase in cytostome number would be expected if actin impacted only late stages of cytostome development. Actin may help to recruit protein complexes required for initial perturbation of the PVM/PPM, which aids in the formation of the cytostome invagination, as has been proposed for endocytosis in other systems (Qualmann et al., 2000; Toret and Drubin, 2006; Yarar et al., 2005). Although *P. falciparum* encodes components of the clathrin-coat complex, we did not observe morphological evidence of clathrin association with cytostomes. The current definition of a cytostome relies on the presence of an electron-dense collar; therefore, clathrin could conceivably associate with the PPM during early stages of cytostome formation, prior to the presence of the electron-dense collar. At present, we have no evidence, nor is there evidence in the literature, for a role of clathrin in cytostome formation.

The decreased number of cytostomes observed in JAS- or CD-treated PE may also suggest a role for actin in stabilization of the cytostomes. JAS and CD may inhibit the ability of the PVM/PPM to invaginate, or they could inhibit the invaginations from becoming stable cytostomes, either of which would result in a decrease in cytostome number. The decrease in cortical actin patches at the PVM/PPM following CD treatment (Fig. 5) suggests that dynamic actin structures might be required for the formation and/or stabilization of cytostomes. The decrease in cytostome number caused by JAS treatment may be due to an inhibition of actin dynamics at the PVM/PPM.

Actin dynamics are also essential for later stages of cytostome development. Residual cytostomes were larger and more convoluted following JAS and CD treatment, suggesting that actin plays an important role in regulating cytostome size. Similarly, actin filaments play a role in regulating the size of endocytic invaginations from the plasma membrane. In yeast, growing actin filaments are proposed to elongate endocytic regions of the plasma membrane in preparation for the formation of endocytic vesicles (Smythe and Ayscough, 2006; Yarar et al., 2005). The presence of long actin filaments surrounding these endocytic invaginations indirectly produces structural size limitations. *Pf*actin may play a similar role in cytostome elongation and may have an indirect role in regulating cytostome size and structure. The

short filaments induced with CD treatment could limit the restrictive effects of *Pf*actin on cytostome morphology resulting in larger and more convoluted cytostomes. JAS, however, may stabilize *Pf*actin filaments thereby limiting the size and convolution of the cytostome, as compared with CD, resulting in fewer CS than in CD-treated PE (Table 2). JAS treatment does, however, result in larger and more convoluted cytostomes than those in untreated PE. This result suggests that proper cytostome morphology requires dynamic actin and/or specific localization of *Pf*actin.

We cannot discriminate whether cytostome regulation is due to a direct association of actin with the cytostome or to an indirect role in lateral membrane domains that regulate the structural and functional properties of the cytostome, or to a combination of both. Despite several attempts, using both parasite-specific and pan-actin antibodies, we were unable to reproducibly localize *Pf*actin to cytostomes in untreated PE. We did, however, often localize *Pf*actin to cytostomes in JAS-treated PE by immunoelectron microscopy. We are uncertain as to whether this *Pf*actin localization represents a typical association of *Pf*actin with the cytostome or whether it is a consequence of the JAS-induced cortical *Pf*actin redistribution. The inability to visualize microfilaments within PE has been well documented, and is attributed, in part, to their diminutive length (~100 nm) (Heintzelman, 2006). The short length of *Pf*actin filaments and the large amount of cytosolic *Pf*actin (Fig. 4, Fig. 5B) contribute to the difficulty of localizing *Pf*actin within PE. The small size of the malaria parasite also limits our interpretations of the immunofluorescence images and precludes us from identifying discrete structures associated with *Pf*actin.

We do, however, have indirect evidence that the cytostome collar possesses an actin component. The electron-dense radiating filaments composing the collar (Fig. 3B, Fig. 8C,D) are within the determined length of endogenous *Pf*actin filaments (50–300 nm) (Schmitz et al., 2005). In addition, the ‘mix-fix’, which helps to preserve actin filaments during fixation (Boyles et al., 1985), allowed us to better visualize the composition of the electron-dense collar. We clearly visualized the collar in some PE thin-sections as consisting of two electron-dense rings with what appeared to be radiating filaments spanning between them (Fig. 3, Fig. 8). We do not yet know the composition of the collar or the functional consequences of these structural organizations. Our results also suggest that actin dynamics function at the cytostome neck, because treatment with either JAS or CD results in structural changes in the cytostome collar, as well as in alterations in the cytostome neck diameter. This, along with the presence of more deeply invaginated, convoluted cytostomes, suggests a role of actin in constriction of the cytostome at the PVM/PPM interface, analogous to its function in receptor-mediated endocytosis (Yarar et al., 2005).

The role(s) of actin in hemoglobin transport

In addition to the role of actin in cytostome formation and morphology, our results suggest that actin has a role in hemoglobin translocation to the FV. The stabilization of actin filaments with JAS (Fig. 5A) inhibited hemoglobin deposition in the FV (Fig. 12), whereas CD appeared to have no major effect on this process (Fig. 12). Similar effects were observed in endocytic virion entry into host cells (Eash and Atwood, 2005; Gilbert et al., 2003). JAS markedly inhibited virion infection, whereas actin destabilizers did not. The variable effects

of these actin-targeted drugs suggested either that JAS induced a structural barrier to endocytosis through the stabilization of the cortical actin cytoskeleton or that these late endocytic steps required actin filament turnover, which is inhibited by JAS (Bubb et al., 2000; Visegrady et al., 2004) but not always by CD (Cooper, 1987). Our results are consistent with both of these interpretations.

Importantly, our results suggest a mechanistic separation between cytostome structure and hemoglobin transport to the FV. The perturbation of cytostome structure, as occurred with JAS or CD treatment, does not necessarily inhibit hemoglobin transport to the FV. Although both CD- and JAS-treated PE had perturbed cytostome morphology, only JAS prevented the delivery of hemoglobin to the FV.

Our results also suggest a link between hemoglobin transport and parasite development. When hemoglobin transport to the FV was inhibited with JAS, parasite development was also impaired, whereas CD treatment affected neither of these processes. Further supporting a link between parasite development and hemoglobin transport is the finding that JAS inhibited *P. falciparum* development most significantly at 20–24 hours post-invasion (Fig. 11), which temporally coincides with the commencement of hemoglobin degradation. The observation that JAS treatment at 12–16 hours post-invasion caused a measurable decrease in *Pf*LDH activity suggests that although a FV is not yet visible, hemoglobin ingestion and transport occurs at this early stage of the intraerythrocytic cycle and is important for parasite development.

A new model for hemoglobin transport

Taking all of our results into account, we propose a new hemoglobin transport model (Fig. 13). We hypothesize that small cytostomes (Fig. 2, steps 1–3) mature into larger structures that extend into the parasite cytosol and contact (Fig. 1B), and subsequently fuse with (Fig. 1E), the FV. Although the relationship between the cytostome and the FV has not been empirically established, the prevailing theory is that the FV is formed from the fusion of several cytostome-derived vesicles (Langreth et al., 1978). In this scenario, cytostome formation would precede FV formation. Our finding of cytostomes early in intraerythrocytic *P. falciparum* development (Fig. 1A), prior to the presence of the FV (Yayon et al., 1984), supports this hypothesis.

Cytostomes were often observed in clusters at specific regions along the parasite PVM/PPM interface (Fig. 1B,D, Fig. 2). Slomianny also observed the presence of multiple cytostomes in close proximity in *P. falciparum*-infected erythrocytes (Slomianny, 1990). This arrangement is reminiscent of the site-directed initiation of eukaryotic endocytosis in other systems (Gaidarov et al., 1999). Cytostome clustering may be a result of favorable membrane conditions originating at specific membrane domains in the PVM/PPM, such as lipid rafts. Lipid rafts were proposed to localize to the PVM (Murphy et al., 2004), and have been implicated as initiation sites for endocytosis (Helms and Zurzolo, 2004). It is also possible that membrane-bound proteins may recruit cytostome-formation complexes to localized regions of the PVM and PPM, as was proposed for endocytic vesicle formation in yeast (Walther et al., 2006).

The inhibition of hemoglobin transport to the FV and the redistribution of actin to the parasite periphery following JAS treatment, suggests that actin may be involved with the recognition and/or fusion events between the cytostome and the FV (Step 6, Fig. 4). We hypothesize that fusion between the FV and the cytostome requires the nucleation of new actin microfilaments to stabilize this event, as was proposed in phagolysosome fusion and exocytic vesicle fusion with the plasma membrane (Kjeken et al., 2004; Sokac and Bement, 2006). Thus, JAS may be inhibiting step 6 (Fig. 10, open arrowheads), either directly by inhibiting nascent filament formation or indirectly by causing a relocation of *Pf*actin away from the cytostome-FV interface and to the parasite periphery (Fig. 5B). The observation that CD treatment did not appear to alter the distribution of *Pf*actin within the parasite cytosol and did not inhibit hemoglobin transport to the FV provides further support for the requirement of actin at the cytostome-FV interface.

In addition, JAS may also inhibit the pinching off of the cytostome from the PVM/PPM (Fig. 13, step 6, arrowheads) through the stabilization of *Pf*actin. If JAS affected only translocation of hemoglobin to the FV and not cytostome pinching off, we would expect to observe double-membrane hemoglobin containing-vesicles within the parasite cytosol. However, JAS only reduced the number of cytostomes and perturbed their morphology; it did not cause an accumulation of double membrane hemoglobin-containing vesicles.

The events described in Fig. 13, steps 6 and 7 (cytostome-FV fusion and cytostome pinching off) are most likely rapid, making their visualization very difficult. We have apparently captured intermediates of this fusion event (Fig. 1C,E), in which the delineation between the cytostome and FV membranes was unclear. This fusion event would result in a brief period during which compartment mixing would occur between the FV lumen and the parasitophorous vacuolar space (PVS). Consistent with this model is the recent finding that FV-resident proteases constitute a substantial portion of the soluble contents of the PVS (Nyalwidhe and Lingelbach, 2006). At neutral pH, the majority of these proteases remain inactive in a membrane-bound proform, and only when they localize to an acidic compartment (i.e. the FV) are they cleaved into their mature, soluble, active forms (Dahl and Rosenthal, 2005; Klemba et al., 2004). Based on their molecular weights, many of these FV-resident proteases are in their mature form within the PVS (Nyalwidhe and Lingelbach, 2006), suggesting mixing of the FV luminal contents with the contents of the PVS during steps 5 and 6 in Fig. 13. The V-ATPase responsible for acidifying the FV is present in the parasite surface membranes (Marchesini et al., 2005) and FV-resident proteases were shown to localize to the cytostome (Francis et al., 1994; Klemba et al., 2004). FV components are, therefore, present in membranes contiguous with the cytostome. Given this arrangement, it seems reasonable that the transfer of hemoglobin to the FV does not require vesicles.

Our new model for hemoglobin ingestion and transport to the FV appears to contradict the prevailing model in the field. In a previous investigation (Klemba et al., 2004), evidence for the transport of hemoglobin in double-membrane vesicles to the FV was based on interpretations of single thin-section electron micrographs. Their conclusion that the hemoglobin-containing structures were discrete vesicles is uncertain without further analysis of these structures by serial-sectioning electron microscopy.

Several recent papers investigating the trafficking of the proteases falcipain-2 (Dasaradhi et al., 2007) and plasmepsin-II (Klonis et al., 2007) to the FV concluded that these proteases were transported to the FV in cytostomal vesicles. These investigators based their interpretations on evaluation of fluorescence microscopy of parasites expressing GFP-chimeras. We suggest that the small size of the malaria parasite, and of the structures involved in hemoglobin ingestion and transport, complicates the interpretations of fluorescence data. For instance, Dasaradhi et al. and Klonis et al. concluded that cytostome-derived transport vesicles often appear closely apposed to the PVM/PPM interface (Dasaradhi et al., 2007; Klonis et al., 2007). With the limitations of the fluorescence microscopy technique, it is difficult to determine whether these structures remain attached to the PVM/PPM interface (and may therefore be cytostomes) or are autonomous from the PVM/PPM (and thus may be hemoglobin transport vesicles). In addition, it is very difficult to ascertain the nature (e.g. do these structures contain hemoglobin) and directionality of these ‘vesicles’. Klemba et al. proposed that plasmepsin-II is transported from the ER to the cytostomes via vesicles, following which cytostome-derived vesicles transport this protease to the FV (Klemba et al., 2004). If the fluorescent structures in the parasite that are suggested to be cytoplasmic vesicles are in fact vesicles, it is impossible to determine if they contain hemoglobin and are derived from the cytostome or if they are intermediates in transport between the ER and cytostome or the cytostome and the FV. In fact, Dasaradhi et al. concede that the apparent cytostome-derived transport vesicles they observe may in fact be ER-derived and may not be directly involved with hemoglobin ingestion (Dasaradhi et al., 2007). Thus, our new model for hemoglobin ingestion and transport to the FV does not necessarily contradict the findings in these and other similar investigations, but rather offers an alternative interpretation of their results.

The results we obtained using JAS and CD to investigate the role of actin in hemoglobin ingestion and transport are in good agreement with those described in a recent report by Smythe et al. (Smythe et al., 2007). A major difference lies in the interpretation of the data. Smythe et al. reported an increase in hemoglobin-containing vesicles in the parasite compartment of PE treated with CD or JAS by immunofluorescence or electron microscopy (Smythe et al., 2007). We made similar observations, but because we used serial-sectioning electron microscopy, we were able to determine that the hemoglobin-containing vesicles were in fact part of the cytostomes. Smythe et al. analyzed only single sections and interpreted their results in light of the traditional hemoglobin transport model (Smythe et al., 2007). They also reported that JAS inhibited hemoglobin endocytosis in PE, whereas CD did not. We report that CD makes cytostomes larger and more convoluted, as does JAS, and that only JAS inhibited delivery of hemoglobin to the FV. Thus, the observations in these studies are similar, but the use of serial sectioning in our investigation provides the basis for an alternative interpretation of the data and a new, vesicle-independent model.

Materials and Methods

Parasite culture

P. falciparum FCR3 strain parasites were cultured in vitro, as described previously, using human O^+ erythrocytes and 5% Albumax (Invitrogen) (Trager and Jensen, 2005). Parasites

were synchronized by using gelatin (Goodyer et al., 1994) and sorbitol treatment (Lambros and Vanderberg, 1979), or by using sequential sorbitol treatments during one intraerythrocytic cycle.

Incubation of PE with actin-perturbing agents

Synchronous PE at 1% hematocrit and ~10% parasitemia were incubated at 37°C with either 7 μM JAS (Invitrogen) or 10 μM CD (Calbiochem) for 3 hours (unless otherwise noted) at the desired times in the intraerythrocytic cycle. To analyze hemoglobin transport to the FV, trophozoite stage PE were incubated with the cysteine protease inhibitor E-64 (10 μM; Sigma) for 1 hour, followed by a 3-hour incubation with either JAS or CD and E-64.

Assay to assess parasite development

A parasite-specific *Pf*LDH assay was used to measure parasite development and sensitivity to drug treatment as described previously (Makler et al., 1993). PE were treated with JAS or CD at the designated intraerythrocytic stage, following which PE were analyzed for *Pf*LDH activity. Untreated PE from the same stock culture were grown in parallel and *Pf*LDH activity was measured for comparison to drug-treated PE.

Separation of triton-soluble and triton-insoluble *Pf*actin from PE

Synchronized PE with or without JAS or CD were lysed with 0.01% saponin in PBS (10 mM sodium phosphate, 140 mM NaCl, pH 7.6) and freed parasites were collected by centrifugation at 3000 ***g***. PHEM buffer (60 mM PIPES, 25 mM Hepes, 10 mM EGTA, 2 mM $MgCl_2$, pH 6.9), containing 0.5% Triton X-100, 1% protease inhibitor cocktail (Sigma), 0.5 mM ATP and 1.0 mM DTT, was added to the parasite pellet. Samples were centrifuged at 410,000 ***g*** for 1 hour at 4°C. The supernatant containing G-actin was mixed with an equal volume of 2×SDS-PAGE loading buffer (100 mM Tris pH 6.8, 10% 2-mercaptoethanol, 4% SDS, 10% sucrose and 0.01% bromophenol blue). The insoluble pellets containing F-actin were resuspended in a 1:1 ratio (volume/volume) of lysis buffer and SDS-PAGE loading buffer; with the final volume of the insoluble pellet fraction adjusted to the final volume of the triton-soluble sample. Equal volumes of each sample were loaded and resolved by 10% SDS-PAGE, then separated proteins were transferred to a nitrocellulose membrane.

Western blotting

A rabbit anti-*Toxoplasma gondii* (*Tg*) actin antibody (1:3000; a gift from Dr David Sibley, Washington University, St Louis, MO) and a horseradish peroxidase (HRP)-conjugated goat anti-rabbit secondary antibody (1:10,000; Jackson Laboratories) were used for the immunodetection of *Pf*actin. *Pf*actin was quantified by densitometric analysis using Kodak 1-D software (Eastman Kodak Company).

Electron microscopy

For morphological analysis of intraerythrocytic *P. falciparum*, synchronized PE with or without drug treatment were fixed in 0.1 M phosphate buffer (pH 7.4) containing 3% glutaraldehyde [Electron Microscopy Sciences (EMS)] and 1% tannic acid (EMS). Cells were post-fixed with 2% osmium tetraoxide (OsO_4) in 0.1 M phosphate buffer (pH 7.4),

stained with uranyl acetate and infiltrated with Spurrs (EMS), as described by Taraschi et al. (Taraschi et al., 2003). The resulting blocks were thin sectioned (~80 nm thick) using a Diatome diamond knife on a Leica ultracut UCT plus microtome. Serial thin sections or single thin sections were post-stained with 2.5% uranyl acetate. Images were viewed using a Hitachi 7000 scanning transmission electron microscope (STEM) and recorded on Kodak 4489 film.

Where designated, PE were fixed simultaneously with 1% glutaraldehyde and 1% OsO_4 in 0.05 M phosphate buffer (pH 7.4) on ice for 30 minutes. This fixation method, termed 'mix-fix', is a modification of a procedure that preserves actin structures for electron microscopy analysis (Boyles et al., 1985). Samples were post-stained, embedded in agarose, infiltrated with Spurrs and further processed as described above.

Cryo-immunoelectron microscopy

PE were fixed in 4% paraformaldehyde (EMS) with 0.01% glutaraldehyde (EMS) in 100 mM PIPES buffer for 1 hour on ice and then pelleted into 10% gelatin in PIPES buffer. The pellets were infused with 2.3 M sucrose in PIPES buffer, mounted on cryo pins and frozen in liquid nitrogen. Ultrathin cryosections were cut at −120°C on a Leica Ultracut UCT with a Leica EMFCS cryo kit, and the resulting ribbons were picked up with a mixture of 2.3 M sucrose and 2% methylcellulose in PIPES buffer and deposited onto carbon/formvar-coated Ni grids. The grids were then incubated for 10 minutes in 0.01 M glycine in PIPES buffer and blocked for 20 minutes in 3% BSA in PIPES buffer. The grids were then incubated for 1 hour at room temperature, or overnight at 5°C, with a 1:500 dilution of the anti-*Toxoplasma* actin antibody with no blocker. The grids were incubated for 10 minutes with 3% BSA and then incubated with a 1:30 dilution of an 18-nm colloidal gold-conjugated goat anti-rabbit IgG (Jackson ImmunoResearch Laboratories) in PIPES buffer. The sections were then embedded in 2.5% uranyl acetate and 1% methylcellulose, and examined in a Hitachi 7000 STEM.

Immunofluorescence

JAS- or CD-treated and untreated synchronized trophozoite stage (20–30 hours post-invasion) PE were fixed in PIPES (100 mM PIPES/0.5 mM $MgCl_2$) buffer (pH 7.0) containing 4% paraformaldehyde and 0.01% glutaraldehyde (electron microscopy grade; EMS) following drug treatment. Fixed PE were processed as previously described (Tonkin et al., 2004), except all washes and solutions used PIPES buffer. Anti-*Tg* actin antibody, used to visualize *Pf*actin, and the 677-1 antibody, which labels an epitope in the PVM/PPM (Gormley et al., 1992), were both used at a dilution of 1:700. Alexa Fluor 488 goat anti-rabbit secondary antibody (Invitrogen) and Alexa Fluor 555 goat anti-mouse secondary antibody (Invitrogen) were used at a dilution of 1:1000. Slides were stained with DAPI (Invitrogen), according to the manufacturer's instructions, to visualize parasite nuclei, and mounted with Prolong Gold antifade reagent (Molecular Probes). Images were viewed on a laser scanning confocal microscope (Zeiss LSM510) with a 100× oil objective with a 1.4 numerical aperture, and processed with LSM510 software and Canvas 7 (Deneba). All images were collected using the same optical parameters.

Statistical analysis

Cytostome number—The number of PE for analysis was determined by counting untreated PE until 100 cytostomes were observed. In parallel experiments, PE were treated with JAS or CD and the cytostome number counted in the same number of PE that was required to view 100 cytostomes in untreated PE. Separate untreated parasite cultures were used for the comparison to JAS- or CD-treated PE. For statistical analysis, untreated PE were combined, as there was no significant difference in the number of cytostomes within these preparations. The incidence of cytostomes was modeled using logistic regression with a linear contrast to compare groups (JAS-treated to untreated PE, CD-treated to untreated PE, and CD-treated to JAS-treated PE). Results are reported as odds ratios (OR), 95% confidence intervals and *P*-values. Analysis was completed using Stata 7 software (StataCorp LP).

CS number—The number of PE analyzed was determined as stated above for cytostome number. CS number was counted simultaneously with cytostome number. The number of CS per cell was modeled using a zero-inflated Poisson regression model followed by linear contrasts to compare groups. Results are reported as incidence rate ratios (IRR), 95% confidence intervals and *P* values. Analysis was completed using Stata 7 software (StataCorp LP).

Cytostome neck diameter—Analysis of variance (ANOVA) of cytostome neck diameters was completed in natural log scale to comply with the normal distribution assumption required for this analysis. The natural logarithm transformations provide a means of transforming skewed data to a symmetric, more normally distributed form. As a sensitivity analysis, nonparametric analysis of variance (Kruskal-Wallis test) was also completed for these data. The nonparametric analysis of variance makes no distributional assumptions, basing the computations on ranks of data rather than individual data values.

Post-hoc paired comparisons in the ANOVA model of untreated PE to JAS-treated PE to CD-treated PE (all possible pairs) were completed, with Tukey's correction of *P*-values for multiple comparisons. All tests were two-sided; with $P<0.05$ considered for statistical significance. Analysis was completed in Systat v8 software (Systat Software).

FV containing undigested hemoglobin—The incidence of swollen FV containing undigested hemoglobin was modeled using logistic regression, with linear contrasts to compare groups. Analysis was completed using generalized estimating equations (GEE) to control for the correlation of results within experiments. Thus, reported *P*-values and confidence intervals were adjusted to correct for this correlation. Results are reported as OR, 95% confidence intervals, and *P*-values. Analysis was completed using Stata 8 software (StataCorp LP).

Acknowledgments

We are grateful to Dr David Sibley for providing the anti-*T. gondii* actin antibody, Dr Eiji Nagayasu for assistance with the *Pf*actin isolation protocol, Dr Terry Hyslop for the statistical analysis and Dr Tatyana Svitkina for helpful discussions. This work was supported by National Institutes of Health grant AI041761.

References

Aikawa M, Hepler PK, Huff CG, Sprinz H. The feeding mechanism of avian malarial parasites. J Cell Biol. 1966; 28:355–373. [PubMed: 5914696]

Banerjee, R.; Goldberg, DE. The *Plasmodium* food vacuole. In: Rosenthal, PJ., editor. Antimalarial Chemotherapy: Mechanisms of Action, Resistance, and New Directions in Drug Discovery. Totawa, NJ: Humana Press; 2001. p. 43-63.

Baum J, Richard D, Healer J, Rug M, Krnajski Z, Gilberger TW, Green JL, Holder AA, Cowman AF. A conserved molecular motor drives cell invasion and gliding motility across malaria life cycle stages and other apicomplexan parasites. J Biol Chem. 2006; 281:5197–5208. [PubMed: 16321976]

Boyles J, Anderson L, Hutcherson P. A new fixative for the preservation of actin filaments: fixation of pure actin filament pellets. J Histochem Cytochem. 1985; 33:1116–1128. [PubMed: 3902963]

Bubb MR, Spector I, Beyer BB, Fosen KM. Effects of jasplakinolide on the kinetics of actin polymerization. An explanation for certain in vivo observations. J Biol Chem. 2000; 275:5163–5170. [PubMed: 10671562]

Cooper JA. Effects of cytochalasin and phalloidin on actin. J Cell Biol. 1987; 105:1473–1478. [PubMed: 3312229]

Dahl EL, Rosenthal PJ. Biosynthesis, localization, and processing of falcipain cysteine proteases of Plasmodium falciparum. Mol Biochem Parasitol. 2005; 139:205–212. [PubMed: 15664655]

Dasaradhi PV, Korde R, Thompson JK, Tanwar C, Nag TC, Chauhan VS, Cowman AF, Mohmmed A, Malhotra P. Food vacuole targeting and trafficking of falcipain-2, an important cysteine protease of human malaria parasite Plasmodium falciparum. Mol Biochem Parasitol. 2007; 156:12–23. [PubMed: 17698213]

Dluzewski AR, Mitchell GH, Fryer PR, Griffiths S, Wilson RJ, Gratzer WB. Origins of the parasitophorous vacuole membrane of the malaria parasite, Plasmodium falciparum, in human red blood cells. J Cell Sci. 1992; 102:527–532. [PubMed: 1506432]

Dobrowolski JM, Niesman IR, Sibley LD. Actin in the parasite Toxoplasma gondii is encoded by a single copy gene, ACT1 and exists primarily in a globular form. Cell Motil Cytoskeleton. 1997; 37:253–262. [PubMed: 9227855]

Eash S, Atwood WJ. Involvement of cytoskeletal components in BK virus infectious entry. J Virol. 2005; 79:11734–11741. [PubMed: 16140751]

Field SJ, Pinder JC, Clough B, Dluzewski AR, Wilson RJ, Gratzer WB. Actin in the merozoite of the malaria parasite, Plasmodium falciparum. Cell Motil Cytoskeleton. 1993; 25:43–48. [PubMed: 8390922]

Foti M, Porcheron G, Fournier M, Maeder C, Carpentier JL. The neck of caveolae is a distinct plasma membrane subdomain that concentrates insulin receptors in 3T3-L1 adipocytes. Proc Natl Acad Sci USA. 2007; 104:1242–1247. [PubMed: 17227843]

Francis SE, Gluzman IY, Oksman A, Knickerbocker A, Mueller R, Bryant ML, Sherman DR, Russell DG, Goldberg DE. Molecular characterization and inhibition of a Plasmodium falciparum aspartic hemoglobinase. EMBO J. 1994; 13:306–317. [PubMed: 8313875]

Francis SE, Sullivan DJ Jr, Goldberg DE. Hemoglobin metabolism in the malaria parasite Plasmodium falciparum. Annu Rev Microbiol. 1997; 51:97–123. [PubMed: 9343345]

Gaidarov I, Santini F, Warren RA, Keen JH. Spatial control of coated-pit dynamics in living cells. Nat Cell Biol. 1999; 1:1–7. [PubMed: 10559856]

Gilbert JM, Goldberg IG, Benjamin TL. Cell penetration and trafficking of polyomavirus. J Virol. 2003; 77:2615–2622. [PubMed: 12552000]

Ginsburg H. Some reflections concerning host erythrocyte-malarial parasite interrelationships. Blood Cells. 1990; 16:225–235.

Gligorijevic B, McAllister R, Urbach JS, Roepe PD. Spinning disk confocal microscopy of live, intraerythrocytic malarial parasites. 1 Quantification of hemozoin development for drug sensitive versus resistant malaria. Biochemistry. 2006; 45:12400–12410. [PubMed: 17029396]

Goldberg, DE. Malaria: Drugs, Disease and Post-Genomic Biology. Sullivan, DJ.; Krishna, S., editors. Heidelberg: Springer-Verlag; 2005. p. 275-292.

Goldberg DE, Slater AF, Cerami A, Henderson GB. Hemoglobin degradation in the malaria parasite Plasmodium falciparum: an ordered process in a unique organelle. Proc Natl Acad Sci USA. 1990; 87:2931–2935. [PubMed: 2183218]

Goodyer ID, Taraschi TF. Plasmodium falciparum: a simple, rapid method for detecting parasite clones in microtiter plates. Exp Parasitol. 1997; 86:158–160. [PubMed: 9207746]

Goodyer ID, Johnson J, Eisenthal R, Hayes DJ. Purification of mature-stage Plasmodium falciparum by gelatine flotation. Ann Trop Med Parasitol. 1994; 88:209–211. [PubMed: 8067816]

Gormley JA, Howard RJ, Taraschi TF. Trafficking of malarial proteins to the host cell cytoplasm and erythrocyte surface membrane involves multiple pathways. J Cell Biol. 1992; 119:1481–1495. [PubMed: 1469045]

Heintzelman MB. Cellular and molecular mechanics of gliding locomotion in eukaryotes. Int Rev Cytol. 2006; 251:79–129. [PubMed: 16939778]

Helms JB, Zurzolo C. Lipids as targeting signals: lipid rafts and intracellular trafficking. Traffic. 2004; 5:247–254. [PubMed: 15030566]

Hempelmann E, Egan TJ. Pigment biocrystallization in Plasmodium falciparum. Trends Parasitol. 2002; 18:11. [PubMed: 11850007]

Holzinger A. Jasplakinolide. An actin-specific reagent that promotes actin polymerization. Methods Mol Biol. 2001; 161:109–120. [PubMed: 11190499]

Hoppe HC, van Schalkwyk DA, Wiehart UI, Meredith SA, Egan J, Weber BW. Antimalarial quinolines and artemisinin inhibit endocytosis in Plasmodium falciparum. Antimicrob Agents Chemother. 2004; 48:2370–2378. [PubMed: 15215083]

Kaksonen M, Toret CP, Drubin DG. Harnessing actin dynamics for clathrin-mediated endocytosis. Nat Rev Mol Cell Biol. 2006; 7:404–414. [PubMed: 16723976]

Kjeken R, Egeberg M, Habermann A, Kuehnel M, Peyron P, Floetenmeyer M, Walther P, Jahraus A, Defacque H, Kuznetsov SA, et al. Fusion between phagosomes, early and late endosomes: a role for actin in fusion between late, but not early endocytic organelles. Mol Biol Cell. 2004; 15:345–358. [PubMed: 14617814]

Klemba M, Beatty W, Gluzman I, Goldberg DE. Trafficking of plasmepsin II to the food vacuole of the malaria parasite Plasmodium falciparum. J Cell Biol. 2004; 164:47–56. [PubMed: 14709539]

Klonis N, Tan O, Jackson K, Goldberg D, Klemba M, Tilley L. Evaluation of pH during cytostomal endocytosis and vacuolar catabolism of hemoglobin in Plasmodium falciparum. Biochem J. 2007; 407:343–354. [PubMed: 17696875]

Lamaze C, Fujimoto LM, Yin HL, Schmid SL. The actin cytoskeleton is required for receptor-mediated endocytosis in mammalian cells. J Biol Chem. 1997; 272:20332–20335. [PubMed: 9252336]

Lambros C, Vanderberg JP. Synchronization of Plasmodium falciparum erythrocytic stages in culture. J Parasitol. 1979; 65:418–420. [PubMed: 383936]

Langreth SG, Jensen JB, Reese RT, Trager W. Fine structure of human malaria in vitro. J Protozool. 1978; 25:443–452. [PubMed: 105129]

Makler MT, Hinrichs DJ. Measurement of the lactate dehydrogenase activity of Plasmodium falciparum as an assessment of parasitemia. Am J Trop Med Hyg. 1993; 48:205–210. [PubMed: 8447524]

Makler MT, Ries JM, Williams JA, Bancroft JE, Piper RC, Gibbins BL, Hinrichs DJ. Parasite lactate dehydrogenase as an assay for Plasmodium falciparum drug sensitivity. Am J Trop Med Hyg. 1993; 48:739–741. [PubMed: 8333566]

Marchesini N, Vieira M, Luo S, Moreno SN, Docampo R. A malaria parasite-encoded vacuolar H(+)-ATPase is targeted to the host erythrocyte. J Biol Chem. 2005; 280:36841–36847. [PubMed: 16135514]

Mizuno Y, Makioka A, Kawazu S, Kano S, Kawai S, Akaki M, Aikawa M, Ohtomo H. Effect of jasplakinolide on the growth, invasion, and actin cytoskeleton of Plasmodium falciparum. Parasitol Res. 2002; 88:844–848. [PubMed: 12172817]

Murphy SC, Samuel BU, Harrison T, Speicher KD, Speicher DW, Reid ME, Prohaska R, Low PS, Tanner MJ, Mohandas N, et al. Erythrocyte detergent-resistant membrane proteins: their

characterization and selective uptake during malarial infection. Blood. 2004; 103:1920–1928. [PubMed: 14592818]

Nyalwidhe J, Lingelbach K. Proteases and chaperones are the most abundant proteins in the parasitophorous vacuole of Plasmodium falciparum-infected erythrocytes. Proteomics. 2006; 6:1563–1573. [PubMed: 16470785]

Olliaro P, Castelli F, Milano F, Filice G, Carosi G. Ultrastructure of Plasmodium falciparum “in vitro”. I Base-line for drug effects evaluation. Microbiologica. 1989; 12:7–14. [PubMed: 2654573]

Orjih AU, Ryerse JS, Fitch CD. Hemoglobin catabolism and the killing of intraerythrocytic Plasmodium falciparum by chloroquine. Experientia. 1994; 50:34–39. [PubMed: 8293798]

Pagola S, Stephens PW, Bohle DS, Kosar AD, Madsen SK. The structure of malaria pigment β-haematin. Nature. 2000; 404:307–310. [PubMed: 10749217]

Pinder JC, Gratzer WB. Structural and dynamic states of actin in the erythrocyte. J Cell Biol. 1983; 96:768–775. [PubMed: 6682109]

Pollard TD, Blanchoin L, Mullins RD. Molecular mechanisms controlling actin filament dynamics in nonmuscle cells. Annu Rev Biophys Biomol Struct. 2000; 29:545–576. [PubMed: 10940259]

Poupel O, Tardieux I. Toxoplasma gondii motility and host cell invasiveness are drastically impaired by jasplakinolide, a cyclic peptide stabilizing F-actin. Microbes Infect. 1999; 1:653–662. [PubMed: 10611742]

Qualmann B, Kessels MM, Kelly RB. Molecular links between endocytosis and the actin cytoskeleton. J Cell Biol. 2000; 150:F111–F116. [PubMed: 10974009]

Rudzinska MA, Trager W, Bray RS. Pinocytotic uptake and the digestion of hemoglobin in malaria parasites. J Protozool. 1965; 12:563–576. [PubMed: 5860234]

Saliba KJ, Allen RJ, Zissis S, Bray PG, Ward SA, Kirk K. Acidification of the malaria parasite’s digestive vacuole by a H^+-ATPase and a H^+-pyrophosphatase. J Biol Chem. 2003; 278:5605–5612. [PubMed: 12427765]

Schmitz S, Grainger M, Howell S, Calder LJ, Gaeb M, Pinder JC, Holder AA, Veigel C. Malaria parasite actin filaments are very short. J Mol Biol. 2005; 349:113–125. [PubMed: 15876372]

Scholl, PF.; Tripathi, AK.; Sullivan, DJ. Bioavailable iron and heme metabolism in Plasmodium falciparum. In: Sullivan, DJ.; Krishna, S., editors. Malaria: Drugs, Disease and Post-Genomic Biology. Heidelberg: Springer-Verlag; 2005. p. 293-324.

Schuler H, Mueller AK, Matuschewski K. Unusual properties of Plasmodium falciparum actin: new insights into microfilament dynamics of apicomplexan parasites. FEBS Lett. 2005; 579:655–660. [PubMed: 15670824]

Sherman IW. Amino acid metabolism and protein synthesis in malarial parasites. Bull World Health Organ. 1977; 55:265–276.

Shurety W, Stewart NL, Stow JL. Fluid-phase markers in the basolateral endocytic pathway accumulate in response to the actin assembly-promoting drug Jasplakinolide. Mol Biol Cell. 1998; 9:957–975. [PubMed: 9529391]

Sijwali PS, Rosenthal PJ. Gene disruption confirms a critical role for the cysteine protease falcipain-2 in hemoglobin hydrolysis by Plasmodium falciparum. Proc Natl Acad Sci USA. 2004; 101:4384–4389. [PubMed: 15070727]

Slater AF, Cerami A. Inhibition by chloroquine of a novel haem polymerase enzyme activity in malaria trophozoites. Nature. 1992; 355:167–169. [PubMed: 1729651]

Slomianny C. Three-dimensional reconstruction of the feeding procees of the malaria parasite. Blood Cells. 1990; 16:369–378. [PubMed: 2096983]

Smythe E, Ayscough KR. Actin regulation in endocytosis. J Cell Sci. 2006; 119:4589–4598. [PubMed: 17093263]

Smythe WA, Joiner KA, Hoppe HC. Actin is required for endocytic trafficking in the malaria parasite *Plasmodium falciparum*. Cell Microbiol. 2007; doi: 10.1111/j.1462-5822.2007.01058.x

Sokac AM, Bement WM. Kiss-and-coat and compartment mixing: coupling exocytosis to signal generation and local actin assembly. Mol Biol Cell. 2006; 17:1495–1502. [PubMed: 16436510]

Taraschi TF, Trelka D, Schneider T, Matthews I. Plasmodium falciparum: characterization of organelle migration during merozoite morphogenesis in asexual malaria infections. Exp Parasitol. 1998; 88:184–193. [PubMed: 9562421]

Taraschi TF, O'Donnell M, Martinez S, Schneider T, Trelka D, Fowler VM, Tilley L, Moriyama Y. Generation of an erythrocyte vesicle transport system by Plasmodium falciparum malaria parasites. Blood. 2003; 102:3420–3426. [PubMed: 12869498]

Tonkin CJ, van Dooren GG, Spurck TP, Struck NS, Good RT, Handman E, Cowman AF, McFadden GI. Localization of organellar proteins in Plasmodium falciparum using a novel set of transfection vectors and a new immunofluorescence fixation method. Mol Biochem Parasitol. 2004; 137:13–21. [PubMed: 15279947]

Toret CP, Drubin DG. The budding yeast endocytic pathway. J Cell Sci. 2006; 119:4585–4587. [PubMed: 17093262]

Trager W, Jensen JB. Human malaria parasites in continuous culture. J Parasitol. 1976; 91:484–486.

Visegrady B, Lorinczy D, Hild G, Somogyi B, Nyitrai M. The effect of phalloidin and jasplakinolide on the flexibility and thermal stability of actin filaments. FEBS Lett. 2004; 565:163–166. [PubMed: 15135072]

Walther TC, Brickner JH, Aguilar PS, Bernales S, Pantoja C, Walter P. Eisosomes mark static sites of endocytosis. Nature. 2006; 439:998–1003. [PubMed: 16496001]

Wellems TE, Plowe CV. Chloroquine-resistant malaria. J Infect Dis. 2001; 184:770–776. [PubMed: 11517439]

Wetzel DM, Hakansson S, Hu K, Roos D, Sibley LD. Actin filament polymerization regulates gliding motility by apicomplexan parasites. Mol Biol Cell. 2003; 14:396–406. [PubMed: 12589042]

Yarar D, Waterman-Storer CM, Schmid SL. A dynamic actin cytoskeleton functions at multiple stages of clathrin-mediated endocytosis. Mol Biol Cell. 2005; 16:964–975. [PubMed: 15601897]

Yayon A, Timberg R, Friedman S, Ginsburg H. Effects of chloroquine on the feeding mechanism of the intraerythrocytic human malarial parasite Plasmodium falciparum. J Protozool. 1984; 31:367–372. [PubMed: 6389846]

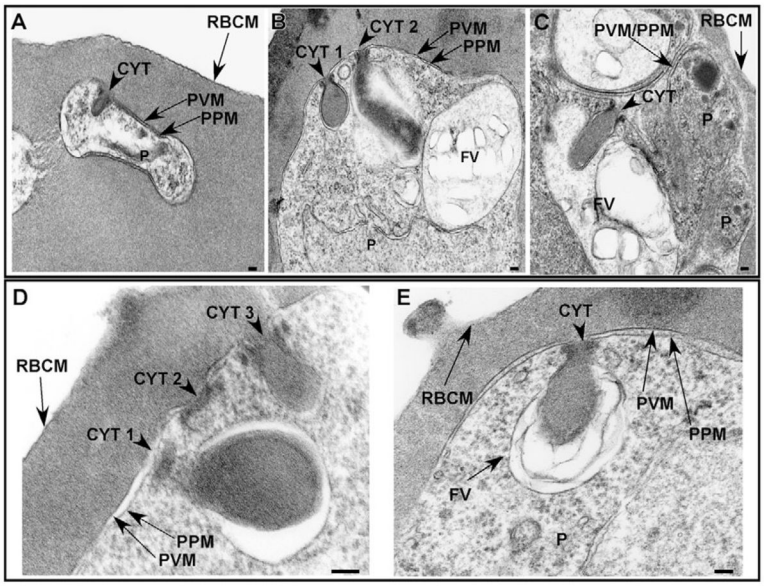

Fig. 1.

Cytostomes are present during each intraerythrocytic stage. (A–C) Electron micrographs depicting the presence of cytostomes (arrowheads) in ring (A), trophozoite (B) and schizont (C) stage parasites. (D) Electron micrograph of a representative trophozoite stage PE in which three cytostomes (CYT) are visible (CYT 1, CYT 2, CYT 3) within a single thin section. (E) Trophozoite stage PE in which the cytostome is observed interacting with the FV. FV, food vacuole; P, parasite; PPM, parasite plasma membrane; PVM, parasitophorous vacuolar membrane; RBCM, red blood cell membrane. Scale bar: 100 nm.

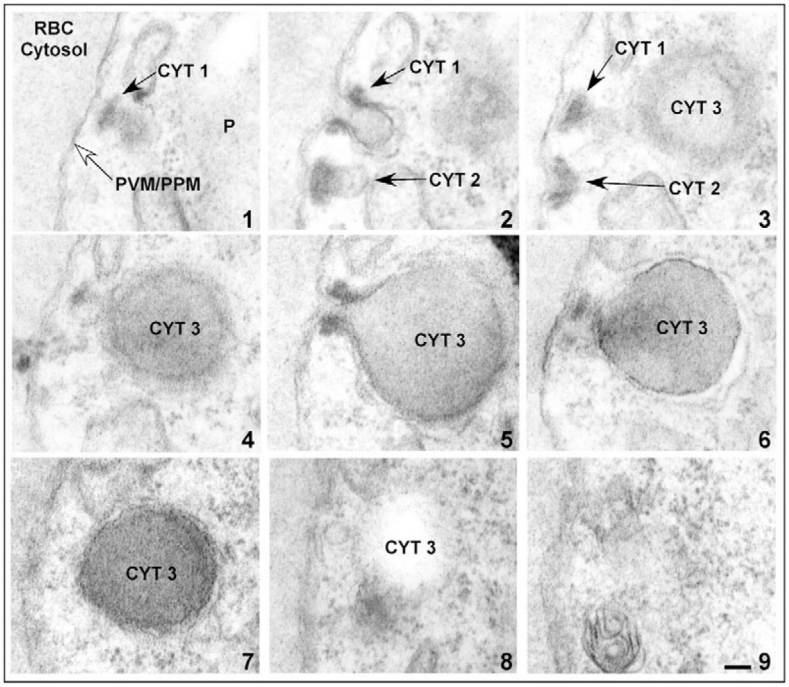

Fig. 2.

Hemoglobin-containing compartments are contiguous with the cytostome. Electron micrographs of serial thin sections (sections 1–9) from a representative trophozoite stage PE. Three cytostomes, CYT 1, CYT 2 and CYT 3, are apparent. CYT, cytostome; P, parasite; RBC, red blood cell; PPM, parasite plasma membrane; PVM, parasitophorous vacuolar membrane. Scale bar: 100 nm.

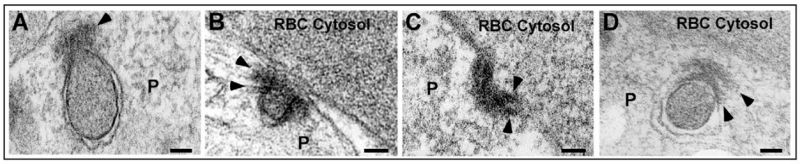

Fig. 3.

Cytostomes possess an electron-dense collar. (A–D) Electron micrographs of representative trophozoite stage PE fixed with ‘mix-fix’. Arrowheads denote the electron-dense collars that encircle the cytostome neck. P, parasite; RBC, red blood cell. Scale bar: 100 nm.

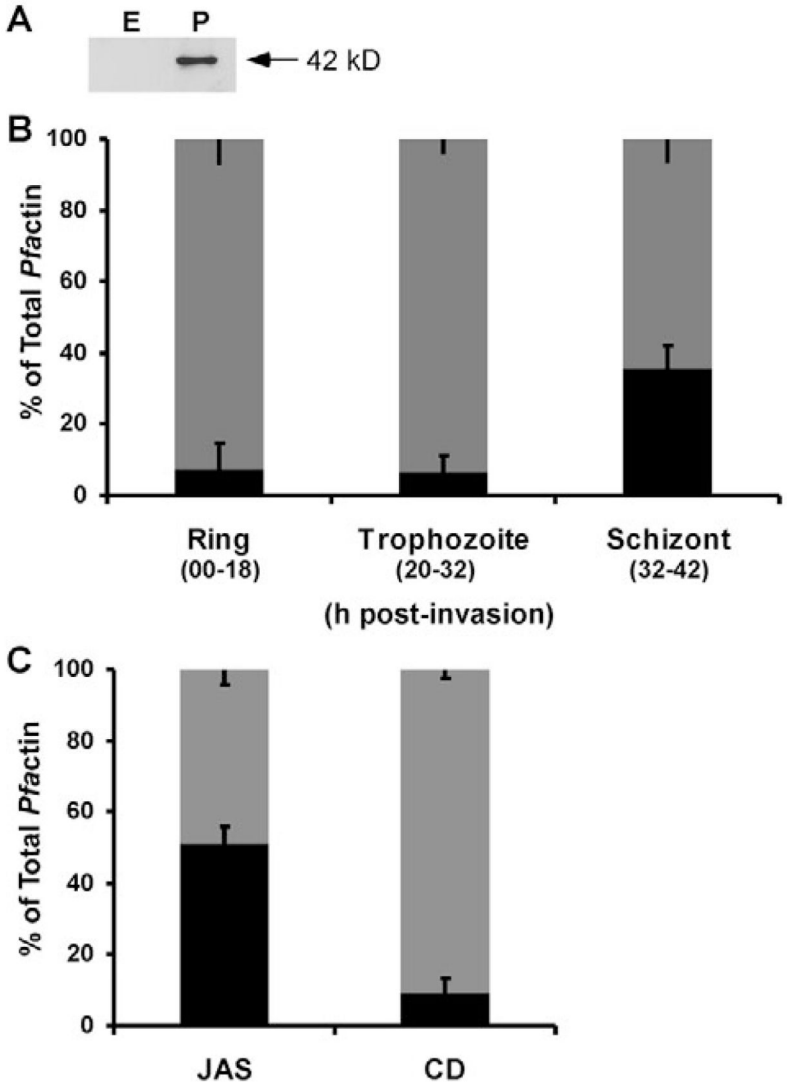

Fig. 4.

Parasite actin distribution in the erythrocytic cycle. (A) Western blot of 15 μg of erythrocyte (E) or parasite (P) protein showing the anti-actin antibody is specific for parasite actin and non-reactive with erythrocyte actin. (B) *Pf*actin in the triton-soluble (gray) and triton-insoluble (black) fractions was quantified by densitometric analysis of western blots using a parasite specific anti-actin antibody in ring (n=4), trophozoite (n=6) and schizont (n=5) stage PE. (C) Triton-soluble (gray) and triton-insoluble (black) *Pf*actin fractions were separated from trophozoites following JAS (n=6) or CD (n=6) treatment, and quantified by densitometric analysis of western blots using a parasite specific anti-actin antibody. Data are expressed as a percentage of total *Pf*actin±s.e.m.

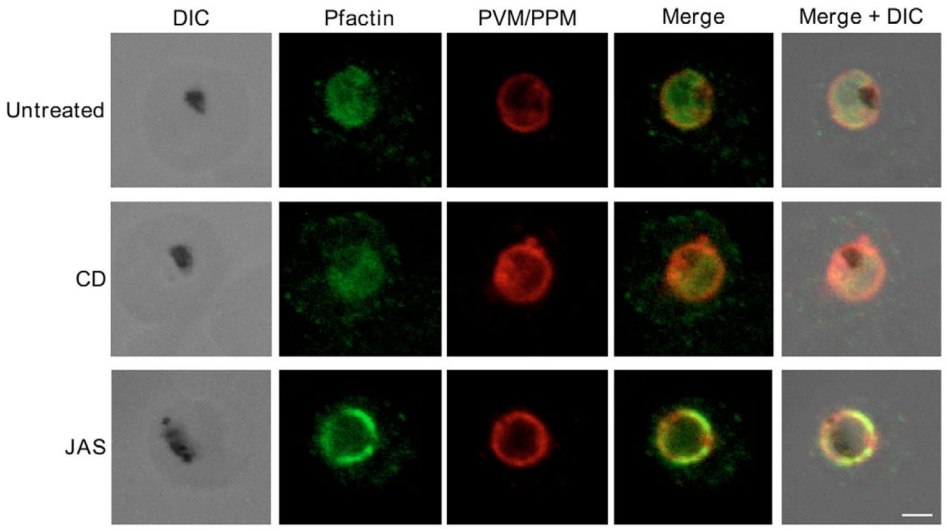

Fig. 5.

*Pf*actin distribution and localization in untreated, JAS- or CD-treated trophozoite stage PE. Representative confocal microscopy images showing *Pf*actin localization (green) in relation to the PVM/PPM (red) in untreated, JAS- and CD-treated trophozoite PE. Merge is a composite of the green and red images; merged+DIC is a composite of the DIC, green and red images. The electron-dense inclusion (hemozoin) in the DIC images indicates the location of the parasite FV. Bar, 2.0 μm.

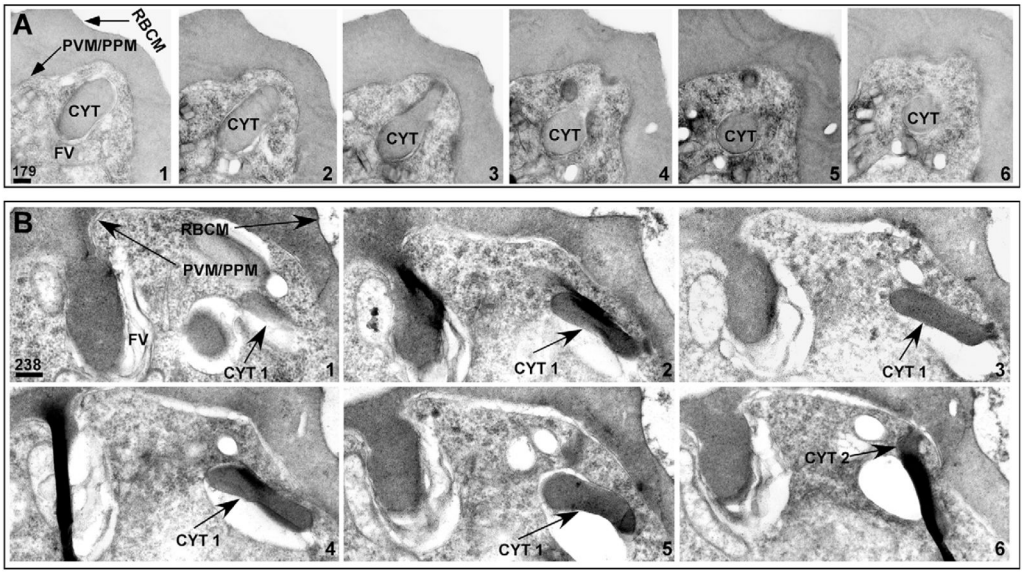

Fig. 6.

Serial-section electron micrographs of JAS- and CD-treated PE. Representative serial thin-section electron micrographs depicting cytostome morphology in (A) JAS-treated and (B) CD-treated PE. Scale bars are in nm.

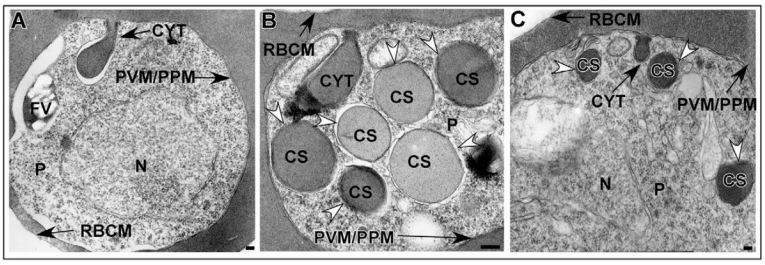

Fig. 7.

Single thin-section electron micrographs of untreated, JAS- or CD-treated trophozoite-stage PE. (A–C) Representative single thin-section electron micrographs of (A) untreated, (B) CD- or (C) JAS-treated PE. White arrowheads denote CS. CS, cytostomal section; CYT, cytostome; FV, food vacuole; N, nucleus; P, parasite; PPM, parasite plasma membrane; PVM, parasitophorous vacuolar membrane; RBC, red blood cell; RBCM, red blood cell membrane. Scale bar: 100 nm

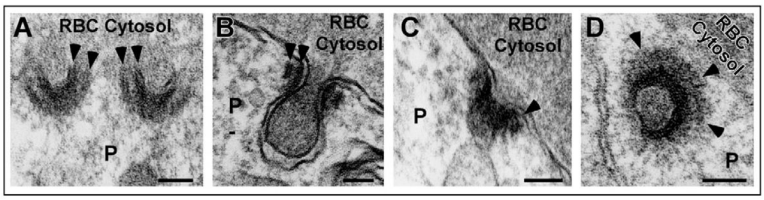

Fig. 8.

Electron micrographs showing cytostome collar morphology in JAS-treated PE. (A–D) Single thin-section electron micrographs of trophozoite PE fixed with ‘mix-fix’ immediately following incubation with JAS. (A,B) The electron-dense ring is observed as two electron-dense collars (arrowheads). Note the radiating electron-dense pattern at the cytostome neck both in the horizontal view (C) and the top view (D). Scale bar: 100 nm.

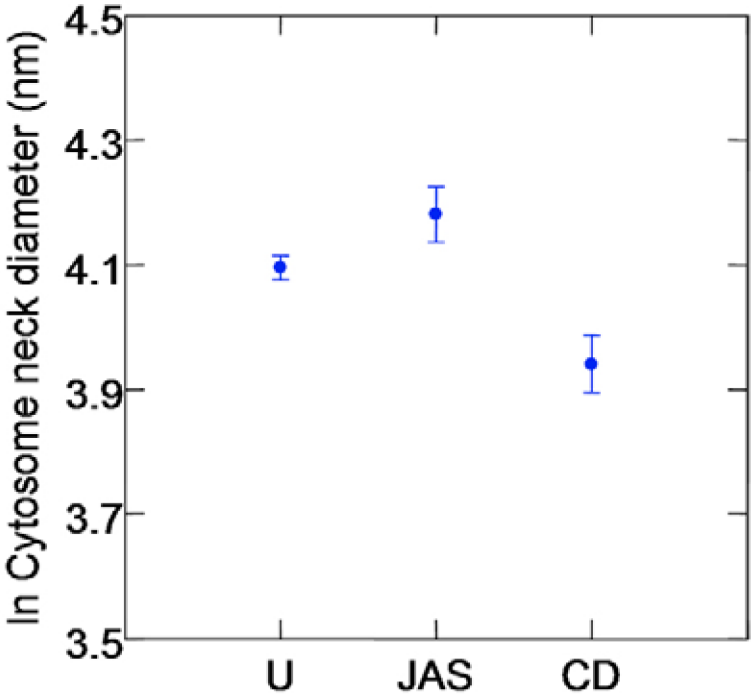

Fig. 9.

The effects of JAS and CD on cytostome neck diameter. Dot plot displaying cytostome neck diameters analyzed in untreated (U; n=103), JAS-(n=47), and CD- (n=41) treated PE. Data are displayed in the natural log scale with the dots representing the means±s.e.m.

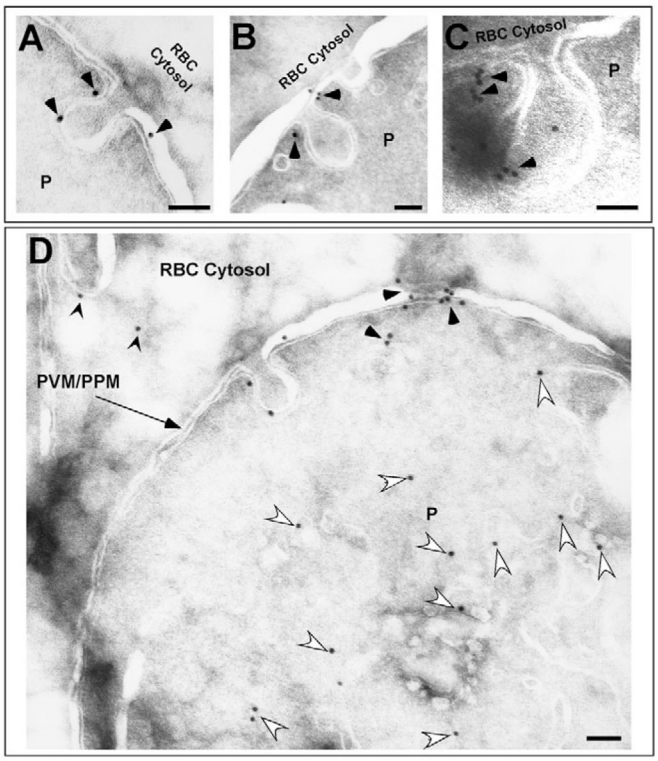

Fig. 10.

Immunoelectron microscopy depicting the localization of *Pf*actin in JAS-treated PE. (A–D) Representative electron micrographs depicting localization of *Pf*actin in JAS-treated trophozoite PE. (A–C) *Pf*actin associated with the neck and body of the cytostome (black arrowheads). (D) *Pf*actin is specifically labeled with the anti-actin antibody in the PVM/PPM (black arrowheads) and the parasite cytosol (white arrowheads). In addition, some *Pf*actin is present in the erythrocyte cytosol (pointed black arrowheads). Scale bar: 100 nm.

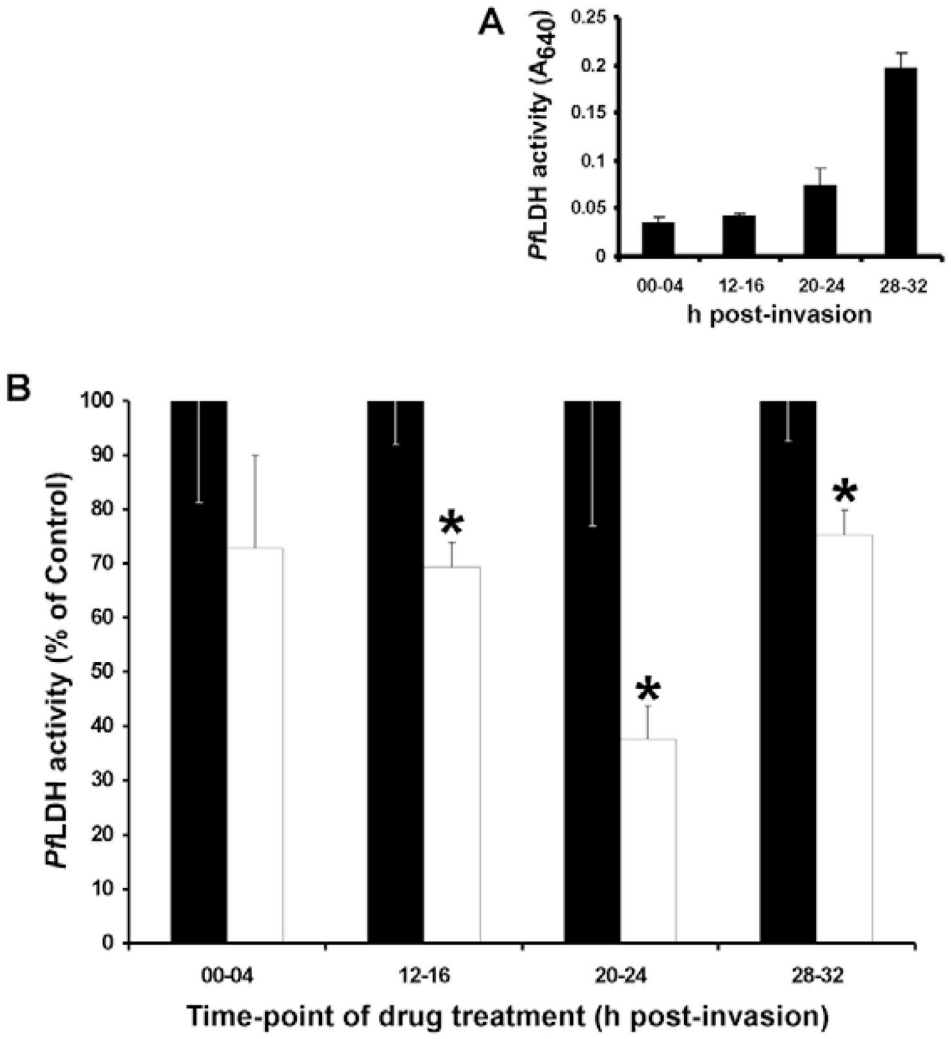

Fig. 11.

The effect of JAS on *P. falciparum* intraerythrocytic development. (A,B) *Pf* lactate dehydrogenase (*Pf*LDH) activity was measured in the ring (00-04 hours post-invasion; n=3), late ring (12–16 hours post-invasion; n=3), early trophozoite (20–24 hours post-invasion; n=3) and late trophozoite (28–32 hours post-invasion; n=3) stages. (B) *Pf*LDH activity was measured following a 3-hour incubation with (white bars) and without (black bars; n=3) JAS. Data are normalized to number of parasites and are expressed as a percentage of *Pf*LDH activity in untreated PE; error bars denote ±standard error. Statistical significance (asterisks) was determined using Student's t-test, where P<0.05 when comparing untreated and JAS-treated PE within each intraerythrocytic stage. n, number of separate parasite cultures analyzed.

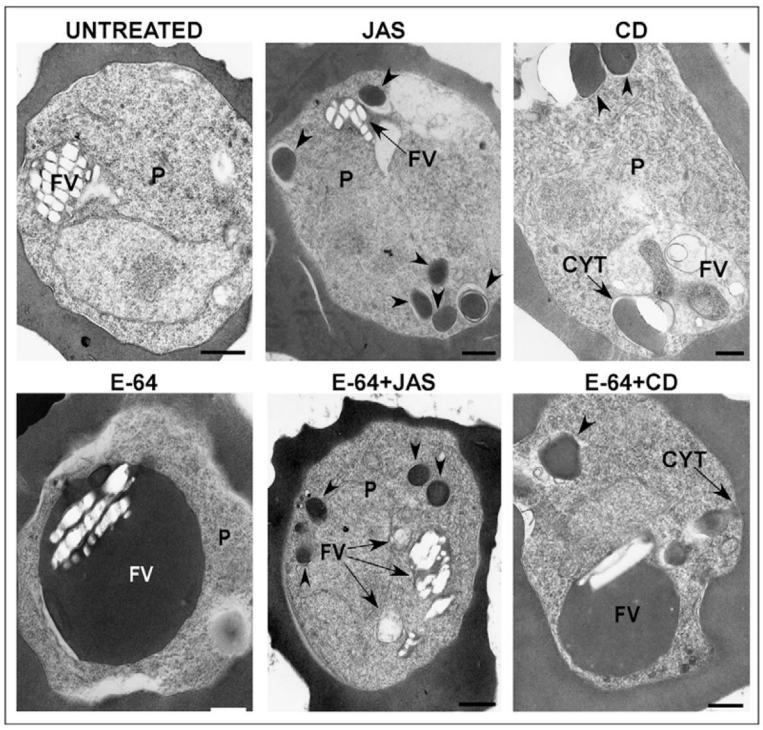

Fig. 12.

Effects of JAS and CD on transport of hemoglobin to the FV. Representative electron micrographs depicting the effects of actin-perturbing agents on accumulation of undigested hemoglobin within the FV. Arrowheads denote cytostomal sections (CS). CD, cytochalasin D; FV, food vacuole; JAS, jasplakinolide; P, parasite. Scale bar: 500 nm.

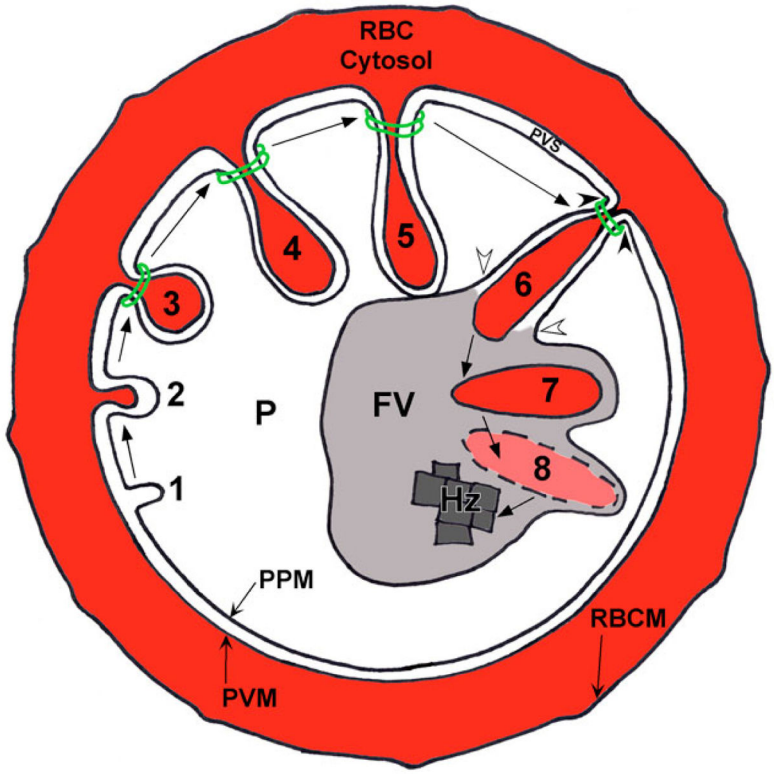

Fig. 13.

A new model for hemoglobin transport to the FV. (Steps 1–3) Cytostome formation. (1) The PVM invaginates after which (2) the PPM invaginates. (3) A double-membrane electron-dense collar forms around the cytostome. (Steps 4–6) Cytostome maturation. (4) The cytostome continues to fill with red blood cell cytosol and hemoglobin, and (5) elongates to appose the FV. (Steps 6–8) Hemoglobin deposition and degradation in the FV. (6) Fusion occurs between the matured cytostome and the FV (white arrowheads), while, simultaneously, the cytostome pinches off from the PVM and PPM (black arrowheads), resulting in the release (7) of a single-membrane-bound hemoglobin-filled vesicle into the FV lumen. During Step 6 (white arrowheads) content mixing occurs between the FV lumen and the PVS. (8) The membrane of this vesicle is degraded by FV-resident lipases, while the hemoglobin is degraded by FV-resident proteases. The resulting heme is polymerized into hemozoin (Hz). P, parasite; PPM, parasite plasma membrane; PVM, parasitophorous vacuolar membrane; PVS, parasitophorous vacuolar space; RBC, red blood cell; RBCM, red blood cell membrane.

Table 1

The effects of actin-perturbing agents on cytostome number

	% *Pf* with cytostomes	Odds ratio	95% confidence interval	*P*-value
Untreated	4.7	Referent	–	–
CD	3.6	0.75	(0.57, 0.99)	0.047
JAS	3.1	0.66	(0.50, 0.99)	0.003
CD versus JAS	–	1.14	(0.81, 1.60)	0.50

A modeled logistic regression quantifying the change in cytostome number following actin-perturbing drug treatment. PE were treated with 7 μM JAS (n=2266), 10 μM CD (n=1916), or were untreated (n=4182). Following a 3-hour incubation, PE were analyzed by electron microscopy. Data are expressed as odds ratios of the incidence of cytostomes in untreated, JAS-and CD-treated PE. Cytostomes were defined as double-membrane invaginations of the PVM/PPM that possessed electron density at their necks. Statistical significance was determined using a linear regression, where $P \leq 0.05$. n, number of PE counted. The n value for untreated PE is the result of combining the count from two separate experiments (i.e. 2266+1916). CD, cytochalasin D; JAS, jasplakinolide; *Pf*, *Plasmodium falciparum*.

Table 2

The effects of actin-perturbing agents on CS number

	% *Pf* with CS	Incidence rate ratio	95% confidence interval	*P*-value
Untreated	26.1	Referent	–	–
CD	63.3	3.66	(3.40, 3.94)	<0.001
JAS	50.5	2.33	(2.07, 2.41)	<0.001
CD versus JAS	–	1.64	(1.53, 1.76)	<0.001

A modeled logistic regression quantifying the change in CS number following actin-perturbing drug treatment. PE were treated with 7 μM JAS (n=2266), 10 μM CD (n=1916), or were untreated (n=4182). Following a 3-hour incubation, PE were analyzed by electron microscopy. Data are expressed as an incidence rate ratio of CS in untreated, JAS- and CD-treated PE. CS are defined as double-membrane, hemoglobin-containing compartments that are not contiguous with the PVM/PPM within a single thin electron micrograph section. Statistical significance was determined using a zero-inflated Poisson regression model, where $P \leq 0.05$. n, number of PE counted. CS, cytostomal section; CD, cytochalasin D; JAS, jasplakinolide; *Pf*, *Plasmodium falciparum*.

Table 3

Descriptive statistics for cytostome neck diameters in original scale

	Untreated	JAS	CD
n	103	47	41
Mean (nm)	65.7	84.5	57.3
Standard deviation (nm)	24.1	28.3	20.6

Descriptive statistics in the original scale of cytostome neck diameters by treatment group (untreated, JAS treated, CD treated). *n*, number of cytostome neck diameters analyzed.

Table 4

The effects of actin-perturbing agents on hemoglobin localization to the FV

	% FV with hemoglobin	Odds ratio	95% confidence interval	*P*-value
E-64	94	Referent	–	–
CD	96	0.77	(0.50, 1.18)	0.231
JAS	20	0.02	(0.01, 0.04)	<0.001
CD versus JAS	–	33.53	(18.91, 59.46)	<0.001

A modeled logistic regression with linear contrasts to compare treatment groups (JAS to untreated, CD to untreated, CD to JAS) of the incidence of swollen FV filled with electron-dense undigested hemoglobin. Significance was determined when $P \leq 0.05$. PE were counted from at least two separate experiments per treatment group ($n=300$). CD, cytochalasin D; FV, food vacuole; JAS, jasplakinolide. *n*, number of PE analyzed.